Biomaterials Science

ROYAL SOCIETY OF CHEMISTRY

PAPER

View Article Online
View Journal | View Issue

Cite this: *Biomater. Sci.*, 2020, **8**, 4287

Three dimensional printed degradable and conductive polymer scaffolds promote chondrogenic differentiation of chondroprogenitor cells

Aruna Prasopthum, †[a,b] Zexing Deng,†[c] Ilyas M. Khan,[d] Zhanhai Yin,[e] Baolin Guo*[c] and Jing Yang *[a,f]

Conductive polymers have been used for various biomedical applications including biosensors, tissue engineering and regenerative medicine. However, the poor processability and brittleness of these polymers hinder the fabrication of three-dimensional structures with desirable geometries. Moreover, their application in tissue engineering and regenerative medicine has been so far limited to excitable cells such as neurons and muscle cells. To enable their wider adoption in tissue engineering and regenerative medicine, new materials and formulations that overcome current limitations are required. Herein, a biodegradable conductive block copolymer, tetraaniline-*b*-polycaprolactone-*b*-tetraaniline (TPT), is synthesised and 3D printed for the first time into porous scaffolds with defined geometries. Inks are formulated by combining TPT with PCL in solutions which are then directly 3D printed to generate porous scaffolds. TPT and PCL are both biodegradable. The combination of TPT with PCL increases the flexibility of the hybrid material compared to pure TPT, which is critical for applications that need mechanical robustness of the scaffolds. The highest TPT content shows the lowest tensile failure strain. Moreover, the absorption of a cell adhesion-promoting protein (fibronectin) and chondrogenic differentiation of chondroprogenitor cells are found to be dependent on the amount of TPT in the blends. Higher content of TPT in the blends increases both fibronectin adsorption and chondrogenic differentiation, though the highest concentration of TPT in the blends is limited by its solubility in the ink. Despite the contradicting effects of TPT concentration on flexibility and chondrogenic differentiation, a concentration that strikes a balance between the two factors is still available. It is worth noting that the effect on chondrogenic differentiation is found in scaffolds without external electric stimulation. Our work demonstrates the possibility of 3D printing flexible conductive and biodegradable scaffolds and their potential use in cartilage tissue regeneration, and opens up future opportunities in using electric stimulation to control chondrogenesis in these scaffolds.

Received 18th April 2020,
Accepted 16th June 2020

DOI: 10.1039/d0bm00621a

rsc.li/biomaterials-science

1 Introduction

Bioelectricity appears in the body and plays an important role in maintaining biological functions such as signal transmission in the nervous system, muscle contraction and wound healing. This fact has promoted the ideal of using electrical stimulations as a potential approach to regulate cellular functions.[1–3] A way to electrically stimulate cells is to use conductive materials to direct the cells that are in contact with these materials to desirable cellular behaviours. To this end, conductive polymers, such as polypyrrole, polyaniline, and polythiophene, have shown the ability to influence cell behaviour such as cell adhesion, proliferation, and differentiation with or without electrical stimulation.[4–7] For example, the inherent piezoelectric properties of bone tissue has led to the

[a]*School of Pharmacy, University of Nottingham, Nottingham, NG7 2RD, UK. E-mail: jing.yang@nottingham.ac.uk*
[b]*School of Pharmacy, Walailak University, Thasala, Nakhon Si Thammarat 80160, Thailand*
[c]*Frontier Institute of Science and Technology, and Key Laboratory of Shaanxi Province for Craniofacial Precision Medicine Research, College of Stomatology, Xi'an Jiaotong University, 10054, China. E-mail: baoling@mail.xjtu.edu.cn*
[d]*Centre of Nanohealth, Swansea University Medical School, Singleton Park, Swansea, SA2 8PP Wales, UK*
[e]*Department of Orthopaedics, The First Affiliated Hospital of Xi'an Jiaotong University, Xi'an, 710061, China*
[f]*Biodiscovery Institute, University of Nottingham, Nottingham, NG7 2RD, UK*
†These authors contributed equally to this work.

investigation of conductive materials for promoting bone repair and osteogenesis.[8] Electrical stimulation with a conductive polymer promoted neurite outgrowth and synaptogenesis of mouse primary neurons.[9] A biohybrid hydrogel containing poly(3,4-ethylenedioxythiophene):polystyrene sulfonate has improved electrical conductivity and prevented arrhythmia of tissue constructs containing neonatal rat cardiomyocytes.[10] Cell and tissue compatibility of these conductive polymers have been demonstrated both *in vitro* and *in vivo*.[11–13] For example, we have shown the *in vivo* biocompatibility of copolymers that contain aniline oligomers in animal testing for myogenic differentiation[14] and wound healing.[15]

One drawback associated with conductive polymers, which hindered their applications in tissue engineering and regenerative medicine, was their inability to degrade. This was solved by rendering conductive polymers with erodibility by grafting hydrophilic pendant groups[16] or biodegradability by combining conductive oligomers with degradable segments, such as aliphatic biodegradable polyesters, to form copolymers.[15,17–19] Degradable and conductive copolymers with different architectures, such as linear, grafted, star-shaped and hyperbranched polymers, have been synthesised.[20,21] The ester bonds in the copolymer endow the ability of hydrolytic degradation. We have demonstrated the degradability of PCL-*co*-aniline oligomer copolymers in our previous study.[22] It has also been shown that the aniline oligomer can be phagocytosed by macrophages.[18] The aliphatic polyester segments are also more flexible than the rigid backbone of conductive oligomers, which improves the flexibility of the copolymer.

Several studies, including some of the author's, have demonstrated the potential of using biodegradable and conductive copolymers to stimulate cell proliferation and tissue repair.[22–25] These studies have been conducted on moulded polymers or electrospun mats. In moulding or electrospinning processes, conductive polymers are first dissolved in organic solvents, and the resulting solutions were then cast[22] or electrospun[25,26] and form solid samples after solvent evaporation. The control over architecture by these techniques is a shortcoming, which limits these materials' use in certain applications. 3D printing is a manufacturing tool which can make 3D objects with controlled overall geometries and internal architectures such as pore size.[27,28] It has been adopted in the tissue engineering and regenerative medicine field to make scaffolds or cell-laden constructs with improved control over positioning of materials and cells in 3D. Many groups including the authors have used 3D printing techniques, such as fused deposition modelling and direct ink writing to fabricate biodegradable polymer scaffolds.[28–31] For example, 3D printed cellular constructs containing decellularized skeletal muscle extracellular matrix have been demonstrated to be responsive to electrical stimulation.[31]

To our knowledge, biodegradable conductive copolymers have not been 3D printed before. We hypothesise that 3D printing can be used to print these conductive copolymers so that their range of architectures can be increased dramatically, which benefits various applications in which these copolymers are utilised. Moreover, the cellular responses on conductive polymers have been mainly focused on neurons[7,32] muscle cells[33–35] and bone cells.[24,36,37] However, there is little information on the potential of these materials on promoting chondrogenic differentiation of mesenchymal stem or progenitor cells. Given the universal presence of bioelectrical signals within various cell types,[3] it is hypothesised that conductive polymers may also have an effect on chondrogenesis of chondroprogenitor cells. In this study we investigated the processing conditions for the direct ink writing of a blend of polycaprolactone (PCL) (M_n = 80 000) and an in-house synthesised conductive copolymer (TPT). The high molecular weight PCL was used to formulate a printable concentrated polymer ink and to improve the ductility of the relatively rigid conductive copolymer. Porous scaffolds with different proportions of the conductive copolymer mixed in the blends were successfully printed. The mechanical properties of these 3D printed scaffolds were measured. The addition of doped conductive copolymer rendered the material surfaces more hydrophilic and with more fibronectin absorption. Additionally, chondrogenic differentiation of ovine chondroprogenitor cells was promoted within the 3D printed scaffolds with the conductive copolymer evidenced by the increased secretion of glycosaminoglycans and collagen II. Initiated by this study, future work will be carried out to understand how the conductive material interacts with chondroprogenitor cells to facilitate function and the role of electrical stimulation.

2 Materials and methods

2.1 Materials

Polycaprolactone (PCL, M_n = 80 000), PCL diol (M_n = 2000), *N*,*N*′-dicyclohexylcarbodiimide (DCC) and 4-dimethylaminopyridine (DMAP) were supplied by Sigma Aldrich. The analytical grade *N*,*N*-dimethylformamide (DMF), diethyl ethyl, dichloromethane (DCM) and camphorsulfonic acid (CSA) were provided by Alfa Aesar.

2.2 Synthesis and characterisation of conductive degradable TPT copolymer

The carboxyl capped tetraaniline (TA) was synthesised according to our previous report.[38] The synthesis of TPT was described as follows. 2.05 g TA and 4 g PCL diol were firstly dissolved in 25 mL anhydrous DMF. Afterward, DCC (2.06 g) and DMAP (1.22 g) were added for initiating a 3-day reaction at room temperature. The reaction solution was precipitated in cold diethyl ethyl after reaction. The obtained precipitation was dissolved in DCM and then filtered to get the filter liquor. The liquor was precipitated and dissolved for 3 times to obtain the final TPT product with a TA content of approximately 33%. The copolymer product was dried for 2 days before structural elucidation by several analytical techniques including a Fourier transform infrared (FT-IR) spectrometry (Nicolet 6700, Thermo Scientific Instrument) with the wavenumbers range of

600–4000 cm^{-1}, ^1H NMR (Bruker Ascend 400 MHz) using DMSO-d_6 as the internal standard solvent, and a UV-vis spectrophotometry (PerkinElmer Lambda 35) with a wavelength range of 250–1000 nm. The TPT doped with CSA was dissolved in DCM prior to monitoring the electrochemical property using the Electrochemical Workstation (CHI 660D Instruments), which contained a platinum-wire auxiliary electrode, a platinum disc working electrode, and a Ag/AgCl electrode at a scan rate of 10 mV s^{-1}.[39,40] The conductivity of TPT (σ, S m^{-1}) was tested by a four-probe method anhin:

$$\sigma = 1/R_s \times t$$

where R_s is the sheet resistance and t is the thickness of the tested samples, respectively.

2.3 Manufacture of conductive 3D printed scaffolds

3D printing ink was formulated by blending of CSA-doped TPT with high molecular weight PCL (M_n = 80 000). The TPT (containing approximately 33% TA content) was grinded and firstly dissolved in 0.5 mL methanol. 4.0 g PCL and 4.0 mL DCM were subsequently added to afford viscous printable polymer inks with 2.5 wt% and 5 wt% TA in the blends, respectively. A 57% w/v PCL/DCM solution was also prepared and used as a control ink (0% TA). Lattice scaffolds (1 × 1 × 0.5 cm^3 or 0.8 × 0.8 × 0.8 cm^3 with 250 μm pores, designed by BioCAD) were fabricated by directly writing the viscous TPT/PCL inks through a tapered tip (25G, 250 μm internal diameter, Adhesive Dispensing UK) using a 3D Discovery printer (regenHU, Switzerland) with a pressure of 4 bar and a printing speed of 8.0 mm s^{-1}. The printed scaffolds were solidified as a result of rapid evaporation of volatile DCM and methanol solvents. Structures of 3D printed conductive scaffolds were visualised by a scanning electron microscope (JEOL JSM-6490LV, UK) and an X-ray micro CT scanner (800 μA, 50 kV, Skyscan 1172, Belgium). The resultant printed scaffolds were used for the subsequent experiments without further doping.

2.4 Surface characterisations

CSA-doped TPT/PCL films containing 0, 2.5 and 5 wt% TA were prepared for the characterisations of surface wettability by contact angle measurements (Optical contact angle, USA KINO Industry, USA) and electrical conductivity using a standard four-point probe technique (Agilent, B2900A digital tester). Fibronectin absorption to the 3D printed conductive porous scaffolds was carried out using our previously published method.[28] In brief, the scaffolds were incubated with 30 μg ml^{-1} fibronectin (Sigma-Aldrich, UK) for 24 hours under the standard cell culture condition. The residual amount of fibronectin in the protein solution was used to calculate the amount of absorbed fibronectin. All characterisations were done in triplicate.

2.5 Thermal behaviour

The crystallinity (X_c) and melting temperature of blended CSA-doped TPT/PCL were investigated by a DSC machine (Q20, TA) in an inert N_2 atmosphere with a flow of 50 mL min^{-1}. The operation condition was programmed as follows: ramp 10 °C min^{-1} from −10 to 80 °C and then ramp 10 °C min^{-1} from 80 to −10 °C. X_c was determined by the melting enthalpy of the blend divided by the melting enthalpy of 100% crystalline polycaprolactone, which is 139.5 J g^{-1}.[41]

2.6 Mechanical properties

The blended CSA-doped TPT/PCL films (200–300 μm thick, 3.0 × 0.6 cm^2) were prepared for tensile testing using an MTS Criterion 43 with a crosshead speed of 5.0 mm min^{-1}. The compressive mechanical properties were measured with a Universal Texture Analyser (TA-HD Plus, Stable Microsystems, USA). For compression testing, 3D printed scaffolds (0.8 × 0.8 × 0.8 cm^3) were compressed in the z-direction with a speed of 0.5 mm s^{-1} to 50% strain. The modulus was calculated from the linear range of the stress–strain curves. At least three specimens ($n \geq 3$) were tested for each sample. The samples were tested in dry state.

2.7 Culture of chondroprogenitor cells

Chondroprogenitor cells were enriched from full-depth chondrocytes isolated from the metacarpophalangeal joint of 15-month-old ewes using an existing method.[42] Briefly, cartilage explants were extracted from the joint under sterile conditions, diced and the subjected to sequential digestion. Following incubation digests were poured through a 40 μm Nitex filter (VWR) to remove large aggregates and leave a single cell suspension. Cells were cultured until they had formed colonies (~7–10 days). Individual colonies were isolated using 4 mm-diameter nylon cloning rings (Sigma) using trypsin and re-plated in a fresh FBS-supplemented medium until confluent. Passaged cells were tested for mesenchymal stem cell plasticity using triple differentiation assays, for chondrogenic, adipogenic and osteogenic differentiation. Cells were frozen using 10% (v/v) DMSO in FBS containing medium and stored at −180 °C until required.

Ovine chondroprogenitor cells were maintained and expanded in a low glucose Dulbecco's modified Eagle's medium (DMEM) with GlutaMAX and pyruvate, supplemented with 10% FBS, 1% antibiotic/antimycotic (AB/AM) solution, and 25 μg mL^{-1} L-ascorbic acid phosphate. 5 ng ml^{-1} basic fibroblast growth factor (bFGF, Gibco AA1-155) and 1 ng ml^{-1} TGFβ_1 (GF111, Merck Millipore) were added to increase the expansion rate. Cells were then harvested and manually seeded onto the 3D printed scaffolds (1.5 × 10^6 cells for each 1 × 1 × 0.5 cm^3 scaffold). The conductive scaffolds were sterilised by soaking in 70% ethanol, followed by washing three times in PBS containing 2% AB/AM and twice in DMEM medium containing 10% FBS and 1% AB/AM. After cell seeding, the chondrogenic differentiation medium (DMEM : F12 (1 : 1) medium with 2% FBS, 1% ITS, 50 μg mL^{-1} L-ascorbic acid phosphate, 40 μg mL^{-1} L-proline, 1% ITS+, 1 mM pyruvate and 10 ng ml^{-1} TGFβ_1 and 100 nM dexamethasone) was added. The medium was changed every 2–3 days over a differentiation period of 28 days.

2.8 Chondrogenic differentiation characterisation

Chondrogenic differentiation was assessed based on the quantification of sulphated glycosaminoglycan (sGAG) and total collagen normalised to DNA and the detection of hyaline-specific type II collagen by immunostaining. Briefly, the constructs, harvested at different times over 28 days, were washed with PBS and digested in 600 μl papain digestion buffer (280 μg ml^{-1} papain, 50 mM EDTA, 5 mM L-cysteine in Dulbecco's PBS pH 6.5, all from Sigma-Aldrich) at 37 °C for 3 days. The clear supernatants of the digested samples were used to measure DNA and sGAG contents using a Quant-iTTM Picogreen® kit (Invitrogen) and 1,9-dimethymethylene blue (DMMB, Sigma-Aldrich) assay, respectively. The total collagen content was quantified using HCL-hydrolysed papain digestive samples and a total collagen assay kit (QuickZyme Bioscience, US). Immunostaining was accomplished using formaldehyde-fixed cross-sectional samples. The sections were incubated with an anti-collagen II antibody (MAB1330, Merck Millipore, UK) and followed by an Alexa Fluor 488-labelled secondary antibody (Abcam, ab150113). Fluorescent images were acquired on a Zeiss 780 confocal microscope.

2.9 Statistical analysis

The quantitative values were reported as mean ± standard deviation (SD). Statistically significant differences were analysed by Wilcoxon Rank-sum test or Kruskal–Wallis One-way ANOVA with Tukey's *post hoc* test. $p < 0.05$ was accepted as significantly different and denoted by *.

3 Results and discussion

3.1 Structural elucidation of the synthesised TPT

The chemical structure of the purified TPT product (3 times purification) was primarily characterised by FT-IR (Fig. 1). There were obvious peaks at the wavenumbers of 1720 cm^{-1} and 1235 cm^{-1} that can be assigned as –CO– and –COO– groups, respectively, for the stretching vibrations of TPT. The peaks at 1598 cm^{-1} and 1509 cm^{-1} were corresponding to quinoid and benzenoid rings for the stretching vibrations of TA moiety, respectively.[22] The cluster peaks <1235 nm in FT-IR spectrum represent the C–O and C–C bonds. The chemical structure of TPT was further confirmed by ^{1}H NMR spectrum. Fig. 2 showed the chemical structure of TPT with the corresponding ^{1}H NMR spectrum: δ = 5.90, 6.93–7.95 (m, Ar–H), δ = 2.72–2.79 (m, $-COCH_2CH_2CO-$), δ = 3.97 (t, $-COOCH_2-$), δ = 0.89, 1.29, 1.53 (m, $-CH_2CH_2CH_2-$), δ = 2.26 (t, $-CH_2COO-$), δ = 3.82, 2.89 (t, $-OCH_2CH_2O-$). The peaks between 5.90, 6.93–7.95 ppm represented the ^{1}H(s) of the benzene and quinone rings whilst the peaks at 2.8 and 2.73 ppm indicated the presence of ^{1}H(s) of $-CH_2CH_2-$ next to the planer ring moieties. Multiple peaks at the 0.89, 1.29, 1.53, 2.26 and 3.97 ppm belonged to the ^{1}H(s) of $-OCH_2CH_2CH_2CH_2CH_2CO-$ within PCL moiety. Peaks at 3.82 and 2.89 belonged to the ^{1}H(s) of $-OCH_2CH_2O-$. There were no detectable peaks that represent impurity according to the NMR results. Indeed, all these characterisations warranted the successful synthesis of TPT.

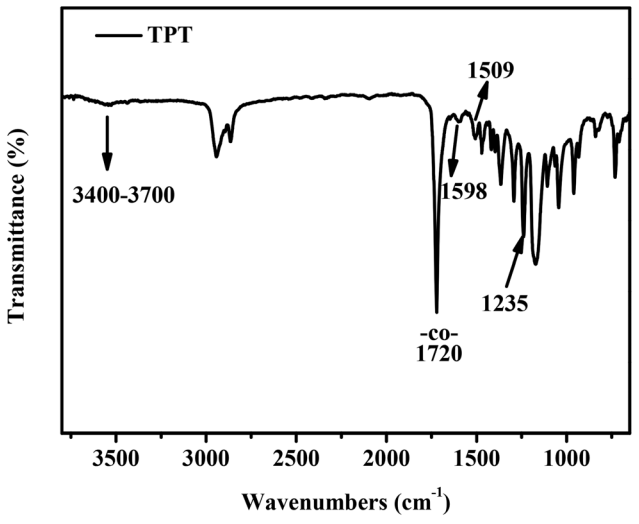

Fig. 1 FT-IR spectrum of tetraaniline-*b*-PCL-*b*-tetraaniline (TPT).

3.2 Electrochemical properties of TPT

The electrochemical properties of TPT were investigated by UV-Vis spectroscopy (Fig. 3A) and cyclic voltammetry (Fig. 3B). The undoped TPT showed the peak of benzene ring (due to π–π transition) at 318 nm and the maximum absorption peak at 590 nm, which was a result of the excitonic transition of benzenoid to quinoid, indicating the insulating emeraldine base (EB) state.[43] After doping TPT with camphorsulfonic acid (CSA), a stable and non-cytotoxic dopant, the peak at 590 nm was almost disappeared whilst the peak at 436 nm appeared, indicating emeraldine salt (ES) state. Moreover, there was a blue shift of the benzene ring peak from 318 to 294 nm.[44] The electrochemical properties of TPT were further investigated by cyclic voltammetry test. There were two regular obvious oxidation/reduction peaks displayed at 0.38 V and 0.58 V, which represented the state transitions from fully reduced leucoemeraldine to half-oxidised emeraldine base and fully-oxidised pernigraniline.[45] The result from the four-probe test revealed that the electrical conductivity of TPT was 6.2×10^{-6} S cm^{-1}.

3.3 Fabrication of 3D printed conductive scaffolds

Several studies have demonstrated the use of biodegradable aniline oligomers for creating tissue-engineered 3D scaffolds, in which the scaffold fabrication methods were limited to thermally-induced phase separation[24,43] and electrospinning.[26,46] Other conductive polymer/hydrogel-matrix composites have used carbon black,[47] carbon nanotubes[48,49] and graphene.[50] However, the conductive components incorporated in polymers or hydrogels were not biodegradable, which could trigger chronic inflammatory responses leading to failure of tissue regeneration and the requirement of surgically removing of the failed scaffolds. Regarding to polymer degradation, we have synthesised a biodegradable block copolymer, TPT, in which tetraaniline (TA) was tethered with aliphatic PCL seg-

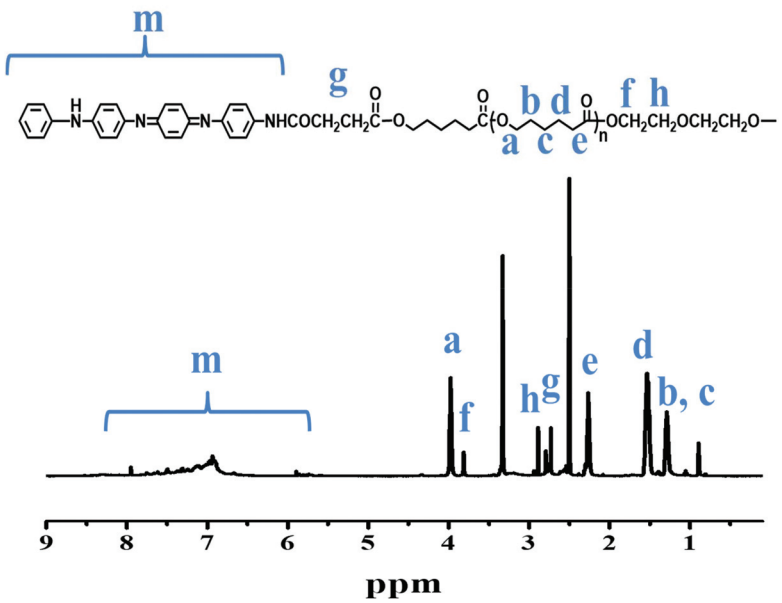

Fig. 2 ^{1}H NMR spectrum of tetraaniline-*b*-PCL-*b*-tetraaniline (TPT) in DMSO-d_6.

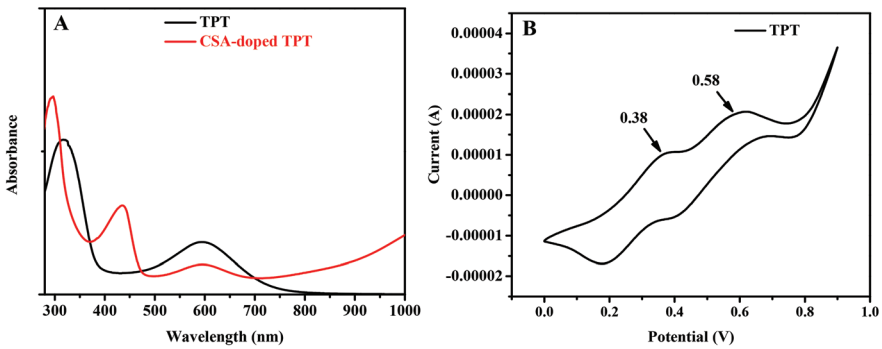

Fig. 3 (A) UV-vis spectra of undoped and CSA-doped TPT in DMSO. (B) Cyclic voltammetry curve of TPT doped by CSA in DMSO solution.

ments *via* biodegradable ester linkages to permit hydrolytic degradation.[22] CSA-doped TPT was blended with high molecular weight PCL (M_n = 80 000) to formulate a viscous polymer ink, enabling the processing of the biodegradable conductive polymer by direct-ink writing, for the first time, into a 3D printed scaffold. The structure of conductive 3D printed PCL scaffold possessed relatively smooth surface struts (an average diameter of *ca.* 85 μm) and 100% interconnected macropores (an average pore size of *ca.* 350 μm), confirmed by micro CT (Fig. 4).

The direct-ink writing process consists of direct extrusion of a viscous polymer solution through a small nozzle to create a 3D object which subsequently solidifies by the evaporation of volatile solvent.[29] The formulation of a printable viscous ink required high concentration of TPT in DCM. However, the synthesised TPT possessed relatively poor solubility in DCM. To afford high-concentration viscous inks for direct-ink writing, CSA-doped TPT was blended with high molecular weight PCL (MW ~80 000 Da). The maximum mass ratio of 17 : 100/TPT : PCL (comprised ~5% TA content) was achieved in our printing ink formulations, which used 1 : 9/methanol : DCM as a solvent, permitting a direct-ink writing of the viscous inks without needle clogging caused by undissolved TPT materials. The printable polymer inks developed herein were homogeneous as confirmed by the presence of a smooth strut surface and the absence of undissolved pieces of the materials inside the strut cross-section (Fig. 4B).

The thermal behaviour of blended TPT/PCL was investigated by DSC. PCL with 2.5% and 5% TA exhibited decreased melting temperatures in a concentration-dependent manner compared to pure PCL (from 64.3 °C to 59.8 °C and 57.9 °C, respectively) (Fig. 5A). Moreover, the apparent crystallinity was also decreased with the increasing amount of TA (33.6%, 29.0% and 27.4% for 0%, 2.5% and 5% TA, respectively). This suggested that the AT segments interfere the crystallisation of the copolymers and PCL. To evaluate whether TA at 2.5% and 5% content in PCL scaffolds was able to elicit electrical conductivity, the printing inks were processed into thin sheets,

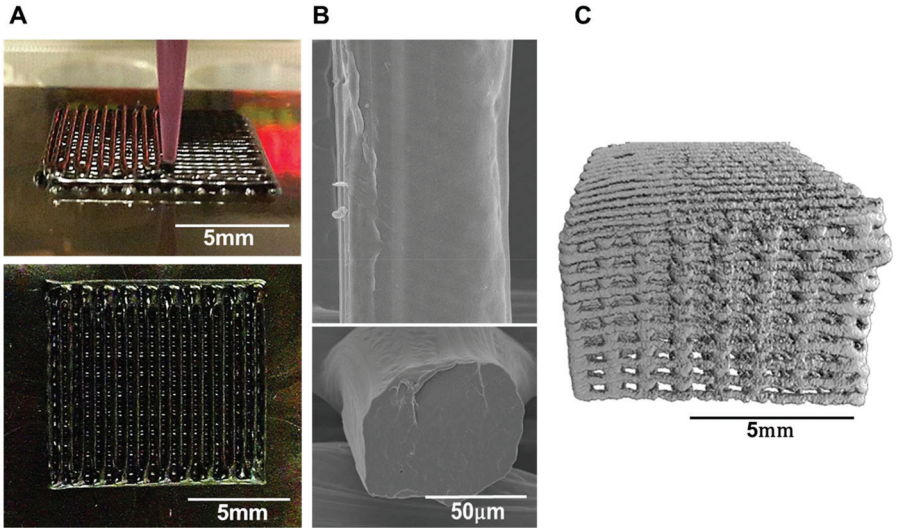

Fig. 4 (A) Images of a 3D printed biodegradable conductive PCL scaffold with 5% TA content. (B) SEM images show strut surface and cross-section. (C) The 3D reconstructed image from micro CT shows well-defined interconnected macropores.

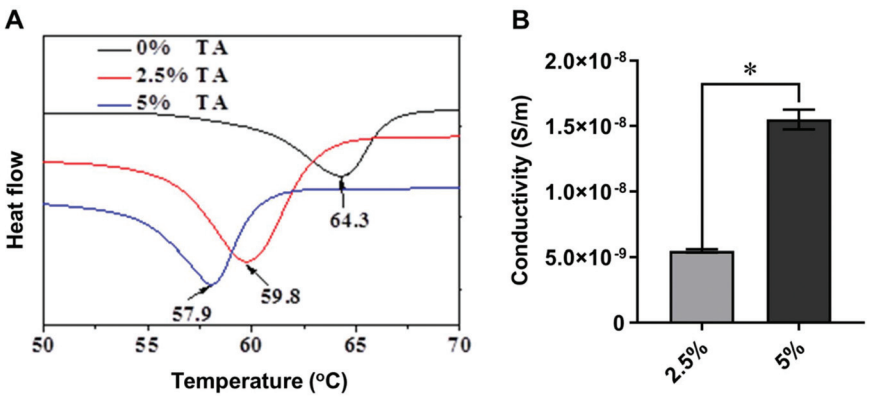

Fig. 5 (A) DSC curves and (B) the conductivity of TPT/PCL blends with 2.5% and 5% TA content. Value represents mean ± SD (n = 3) (*p < 0.05).

and their conductivities were measured by a four-probe analyser (Fig. 5B). Increased conductivity was observed with an increased TA content: 5.48×10^{-9} S m^{-1} for TA content of 2.5% *versus* to 1.55×10^{-8} S m^{-1} for TA content of 5%, indicating that PCL with 2.5% and 5% AT conducted measurable electrical current. This warranted the use of the obtained 3D printed scaffold for investigating the effects of the conductive materials on stem cell differentiation.

3.4 Mechanical properties

An effective way to overcome poor processability of conductive polymers is to mix them with other polymers that have better mechanical properties such as flexibility (*e.g.*, PLLA and PCL) whilst endow conductivity to otherwise insulating polymers.[51,52] In this study, TPT/PCL blends were therefore evaluated for their mechanical properties compared to the pristine PCL (0% TA) using both tensile and compression tests.

Films prepared from casting of TPT/PCL inks were used in tensile tests to determine the mechanical properties that intrinsically depended on material composition. The results in Table 1 and Fig. 6 showed that the tensile strength of PCL decreased with increased TA content (from 26.1 MPa in 0% TA

Table 1 Mechanical properties of PCL (0% TA) and TPT/PCL blends containing 2.5% and 5% TA content. Value represents mean ± SD (n = 3 for tensile, n = 4 for compression)

	Thin sheet (n = 3)			3D printed scaffold (n = 4)
Sample	Tensile modulus (MPa)	Tensile strength (MPa)	Elongation at break (%)	Compressive modulus (MPa)
0% TA	188.6 ± 8.3	26.1 ± 1.9	600.7 ± 47.3	6.8 ± 2.3
2.5% TA	159.2 ± 12.1	18.2 ± 0.9	526.5 ± 29.9	14.7 ± 3.6
5% TA	153.4 ± 4.8	11.7 ± 2.3	77.9 ± 7.5	35.1 ± 9.7

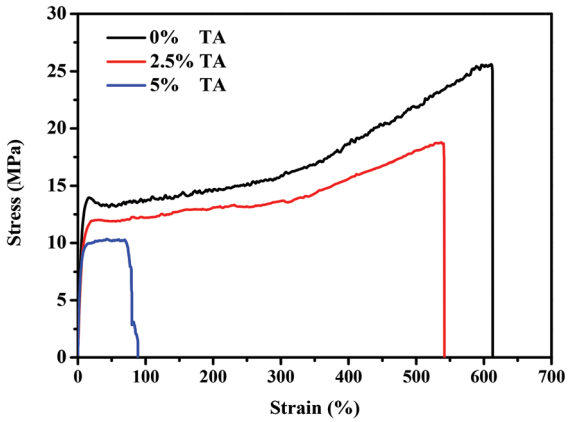

Fig. 6 The representative stress–strain curves of PCL (0% TA) and TPT/PCL blends containing 2.5% and 5% TA content from tensile testing.

to 11.7 MPa in 5% TA). More TA content appeared to render the material more brittle, as indicated by decreased strain at break (from 600.7% strain for 0% TA to 77.9% strain for 5% TA). The pristine PCL (0% TA) showed the highest modulus, tensile strength and strain at break. Decreased strength and strain at break in a TA concentration-dependent manner could be due to the decrease in crystallinity of PCL perturbed by TA moieties.

Compression test was employed to examine the mechanical stiffness of 3D printed porous TPT/PCL scaffolds. The compressive modulus of 3D printed scaffolds seemed to increase in correlation with TA content (from 6.8 MPa for 0% TA to 35.1 MPa for 5% TA, Table 1). In contrast, this trend was not found for the tensile moduli. The differences in modulus values between tensile and compression tests may arise from a combination of the stiff nature of TPT and the different ways of testing. As the TPT components are much stiffer than PCL, they withstand more force under compression than in tensile testing. In tensile testing, the stiffer components are pulling away from each other whilst in compression they are pushed together, hence generating higher modulus from compression testing. As the 3D printed scaffolds were porous (~40% infill density measured by micro CT), they would show decreased moduli compared to thin sheets. However, TPT/PCL blends containing 2.5% and 5% TA were still sufficiently robust and stiff for a variety of tissue engineering applications including cartilage, which has a compressive modulus in the range of 0.44 to 20.4 MPa.[53]

3.5 Surface wettability and fibronectin absorption

To test the effect of TA on the surface chemistry of PCL, we conducted a contact angle measurement to primarily determine the surface hydrophilicity of both CSA-doped and undoped TPT/PCL films with different TA contents (0%, 2.5% and 5%). Flat films were used in this case to allow contact angle measurements without the interference of macropores in the 3D printed scaffolds. The undoped films were used as controls, which have been known to be resistant to protein adsorption due to the formation of a gas–liquid interface caused by hydrophobic effect.[54] For the undoped TPT/PCL films, increased TA content was associated with increased water contact angle from 76.8° (0% TA) to 79.4° (2.5% TA) and 87.7° (5% TA). After doping with CSA, the water contact angle decreased from 76.8° (0% TA) to 63.0° (2.5% TA) and 70.0° (5% TA) (Fig. 7A). Shift of the surface chemistry towards the hydrophilic end was attributed to the protonation of the imine nitrogen atoms in emeraldine base caused by a CSA dopant.[55]

Adsorption of fibronectin, a cell-adhesion promoting ECM protein, to surfaces of implantable 3D printed scaffolds plays a role in regulating concomitant cell responses and in initiating material integration with surrounding tissues.[54,56] In light of this, how the conductive TA domains influence fibronectin absorption onto 3D printed scaffolds was investigated. Fig. 7B showed improved fibronectin absorption for the 3D printed PCL scaffolds with 2.5% and 5% TA when compared to those with 0% TA. It was previously known that increased TA content significantly increased adsorption of proteins from fetal bovine serum (FBS), which is a source of different proteins including fibronectin.[24] However, there was a previous finding

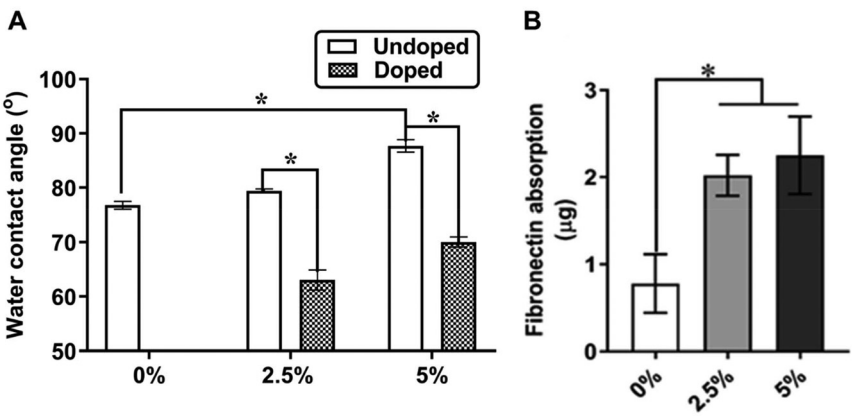

Fig. 7 (A) Surface wettability of thin PCL films with 0%, 2.5% and 5% TA measured by contact angle method. (B) Fibronectin absorption of the 3D printed PCL scaffolds with 0%, 2.5% and 5% TA. Value represents mean ± SD (n = 3) (*p < 0.05).

that showed no correlation between increased TA content and improved fibronectin absorption, but rather conformational changes.[26] The contradiction in fibronectin absorption may be attributed to the varying spatial distribution of entrapped dopants and surface topography differences among the studies as well as the use of different scaffold systems: 3D printed scaffolds *vs.* electrospun mats in the previous study.

3.6 Chondrogenesis of chondroprogenitors in 3D printed conductive scaffolds

Bioelectricity has long been well known to involve in physiological processes including membrane depolarisation to generate nerve impulses, muscle contraction or the release of synaptic vesicles.[3,57] Recent evidence has shown that cells during embryonic development and regenerative repair also respond to bioelectric signals,[2,3] paving the way for conductive polymers to be used in various tissue engineering applications.[6–8] In addition to excitable neurons and muscle cells, bone and stem cells have also been shown to respond to conductive polymers, initiating our exploration of the potential use of conductive polymers for controlling stem/progenitor cell differentiation. For instance, polypyrrole, pyrrole-grafted PCL, aniline oligomer-grafted polylactide and PCL have previously been shown to enhance osteogenic differentiation of mesenchymal stem cells (MSCs).[24,26,58,59] A recent study has reported that electrical stimulation induces chondrogenic differentiation of MSCs (cultured as micromass) by modulating intracellular Ca^{2+}/ATP oscillations.[60] However, the impact of conductive materials including TPT on the differentiation of stem cells down the chondrogenic lineage is yet unknown.

Herein, our study is the first to show the effect of conductive material in the form of 3D printed scaffolds on the chondrogenic differentiation of chondroprogenitor cells, which are present in adult cartilage and are predisposed to specifically differentiate into chondrocytes.[61,62] Chondroprogenitor or chondrocyte-derived progenitor cells are capable of self-renewal similar to MSCs whilst exhibiting less or no expression of RUNX2, the key transcription factor for hypertrophic differentiation: a process thereby inducing the formation of calcified cartilage and bone.[52] Due to their differentiation specificity and resistance to hypertrophy, articular chondroprogenitors have been proposed as promising cell sources for cartilage therapy. Both MSCs and chondroprogenitors have the trilineage differentiation potential.[53,54]

To demonstrate the benefit of conductive TA in promoting chondrogenesis of chondroprogenitors, 3D printed PCL scaffolds ($1 \times 1 \times 0.5$ cm^3, 250 μm macropores) with different TA content (0%, 2.5% and 5%) were seeded with chondroprogenitors (1.5×10^6 cells per scaffold). The cell-seeded scaffolds were cultured over a 28-day period in the chondrogenic differentiation medium containing $TGF\beta_1$ and were harvested at different cultivation times (3 hours, 7, 14 and 28 days). Based on the DNA quantification (Fig. 8A), the presence of TA (2.5% and 5% compared to 0%) appeared to increase chondroprogenitor cell adhesion at 3 hours after cell seeding although no quantitative significant difference was found. The scaffolds with 2.5% and 5% TA showed no cytotoxic effect on chondro-

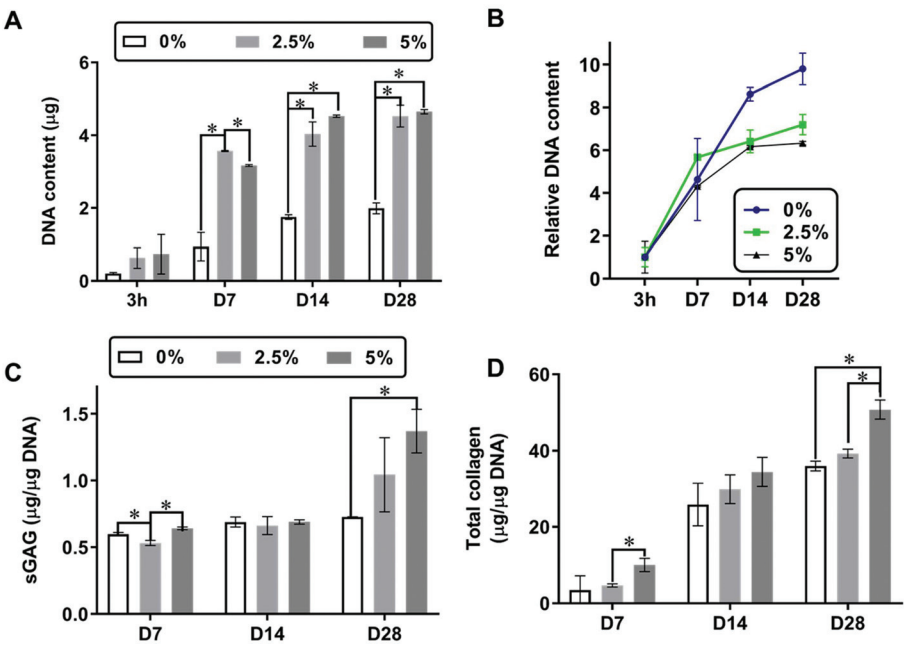

Fig. 8 (A) The absolute and (B) relative DNA content showed the proliferation of primary ovine chondroprogenitor cells on the 3D printed scaffolds with 0%, 2.5% and 5% TA. The relative DNA content was calculated by normalising all DNA content data to the DNA content at 3 h after initial cell seeding. The chondrogenic differentiation of chondroprogenitors in 3D printed PCL scaffolds with 0%, 2.5% and 5% TA characterised by (C) sGAG and (D) total collagen production normalised to DNA. Value represents mean ± SD (n = 9) (* $p < 0.05$).

progenitor cells as significant cell proliferation was observed over the culture period (Fig. 8A). The proliferation profiles were shown in Fig. 8B, by normalising absolute DNA contents of days 7, 14, and 28 to 3 hours. Within the first week of cultivation (3 h-D7), chondroprogenitor cells in 3D printed scaffolds with 2.5% TA entered logarithmic growth phase and reached the stationary phase faster than those in the scaffolds with 5% and 0% TA, respectively (Fig. 8B). It could be seen that the incorporation of 2.5% TA was optimal to induce the proliferation of chondroprogenitor cells as 5% TA showed slower proliferation. However, enhanced sGAG (Fig. 8C) and collagen (Fig. 8D) at day 28 were obtained within the scaffolds with 5% TA, when compared to 0% and 2.5% TA. The cells in 3D printed scaffolds with 2.5% TA exhibited similar amounts of sGAG and total collagen to those on the scaffolds with 0% TA, suggesting that 2.5% TA was not enough to promote chondrogenesis. Fig. 9 showed the representative cross-sectional images of the cell-seeded scaffolds at day 28. Aggregation of cells were observed on the struts regardless of AT percentages (Fig. 9A). The cells expressed type II collagen, a marker of hyaline cartilage, as detected by immunostaining (Fig. 9B). However, the scaffolds with 5% AT appeared to have more type II collagen compared to 0% and 2.5% AT, suggesting increased chondrogenesis (Fig. 9A). This finding indicated that the chondrogenesis of chondroprogenitors were influenced by the presence of the conductive polymer and suggested the potential use of the conductive polymer in cartilage tissue engineering. The underlying mechanisms of how the incorporated conductive TA domains trigger chondrogenesis remains to be elucidated in the future, so does the effect of external electrical stimulation on cell differentiation within the conductive scaffolds.

Overall, our study has firstly demonstrated a simple and facile 3D printing method which allows the fabrication of degradable conductive 3D scaffolds with well controlled geometry. PCL with 5% TA was the optimal content to promote adhesion and chondrogenesis of chondroprogenitor cells. It is hypothesised that the differences in surface chemistry caused by the incorporation of TA could have an effect on spatial distribution of local charges and electrolytes on the strut surfaces of 3D printed scaffold during *in vitro* culture, which could be translated into signal transduction pathways modulating chondrogenic differentiation of chondroprogenitor cells. The native cartilage extracellular matrix is highly electronegative due to the high concentration of negatively charged sulphated glycosaminoglycans covalently attached to proteoglycans, principally aggrecan. Studies have shown the loss of the fixed charge density following cell and tissue injury has deleterious effects leading to osteoarthritic-like changes.[63] The generation of a fixed charge density using electroactive polymers may act as a feedback mechanism to stimulate and modulate proliferation and differentiation of chondroprogenitors. In addition, the modulation of cell ion flows, currents and transmembrane voltages may be other factors that are responsible for the effect of conductive polymers on chondrogenesis. However, illustrating the exact mechanism is a difficult task which needs significant future effort. To illustrate underlying mechanism, it will require the identification of molecular sources of ion flows and its correlations to biochemical and genetic cascades. This will require significant effort in utilising molecular biology

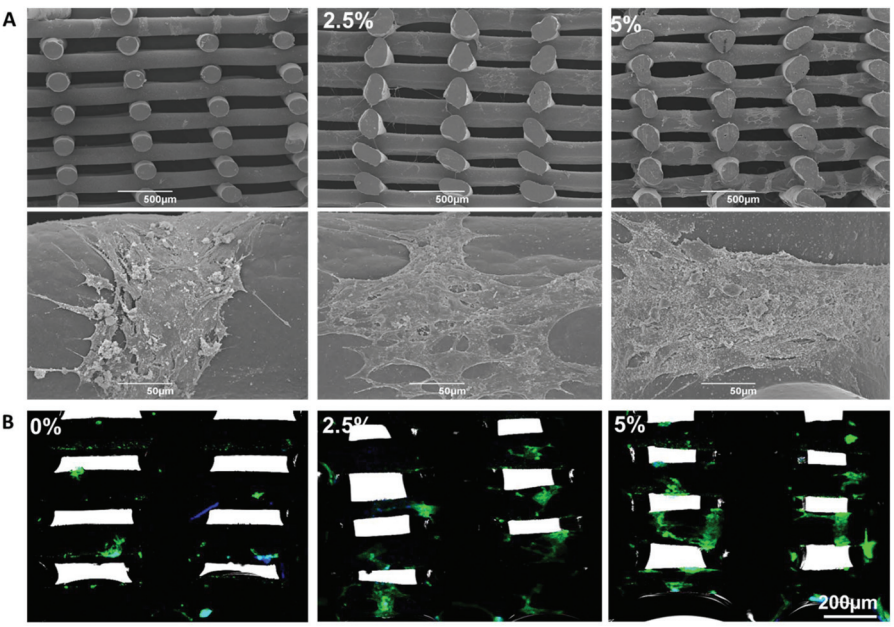

Fig. 9 (A) The representative SEM images showed cell adhesion on the scaffold struts. (B) The representative brightfield-merged confocal fluoresent microscope images showed cross-sections of chondroprogenitor cell-seeded 3D printed PCL scaffolds with 0%, 2.5% and 5% TA at day 28. Positive immunostaining staining of collagen type II was shown as green and nuclei were shown as blue.

and its tools which are currently mainly focusing on biochemical signals to study bioelectric events.

4 Conclusion

Herein, the block copolymer of tetraaniline (TA) and PCL was synthesised and 3D printed for the first time into biodegradable conductive scaffolds. The 3D printed mechanically robust conductive scaffolds were successfully fabricated by direct ink writing of a printable polymer ink, formulated by blending TPT with high molecular weight PCL. The inclusion of the conductive copolymer within the blends rendered electrical conductivity, improved surface hydrophilicity and enhanced fibronectin absorption. We also demonstrated the novel role of conductive polymers in promoting chondrogenic differentiation of chondroprogenitors, which has not previously been explored. Our results have highlighted the potential use of 3D printed biodegradable conductive polymers in cartilage repair. Future work will investigate the effects of electrical stimulation and cartilage regeneration *in vivo* within these conductive scaffolds.

Abbreviations

PCL	Polycaprolactone
3D	Three-dimensional
TA	Tetraaniline
TPT	Tetraaniline-*b*-polycaprolactone-*b*-tetraaniline
sGAG	Sulphated glycosaminoglycans
DMMB	1,9-Dimethylmethylene blue

Conflicts of interest

There are no conflicts of interest to declare.

Acknowledgements

The authors would like to thank Elisa Tarsitano for her help with confocal fluorescence imaging, and the Nanoscale and Microscale Research Centre (NMRC), University of Nottingham for electron microscope facilities. This work was jointly supported by the National Natural Science Foundation of China (grant numbers: 51673155 and 51973172).

References

1 F. Cunha, A. M. Rajnicek and C. D. Mccaig, Electrical Stimulation Directs Migration, Enhances and Orients Cell Division and Upregulates the Chemokine Receptors CXCR4 and CXCR2 in Endothelial Cells, *J. Vasc. Res.*, 2019, **56**, 39–53.

2 C. D. McCaig, A. M. Rajnicek, B. Song and M. Zhao, Controlling Cell Behavior Electrically: Current Views and Future Potential, *Physiol. Rev.*, 2005, **85**, 943–978.

3 M. Levin and C. G. Stevenson, Regulation of Cell Behavior and Tissue Patterning by Bioelectrical Signals: Challenges and Opportunities for Biomedical Engineering, *Annu. Rev. Biomed. Eng.*, 2012, **14**, 295–323.

4 E. Stewart, *et al.*, Electrical stimulation using conductive polymer polypyrrole promotes differentiation of human neural stem cells: A biocompatible platform for translational neural tissue engineering, *Tissue Eng., Part C*, 2015, **21**, 385–393.

5 P. Humpolíček, *et al.*, Stem cell differentiation on conducting polyaniline, *RSC Adv.*, 2015, **5**, 68796–68805.

6 J. Huang, *et al.*, Electrical regulation of Schwann cells using conductive polypyrrole/chitosan polymers, *J. Biomed. Mater. Res., Part A*, 2010, **93**, 164–174.

7 Q. Zhang, *et al.*, Electrical stimulation using conductive polymer polypyrrole counters reduced neurite outgrowth of primary prefrontal cortical neurons from NRG1-KO and DISC1-LI mice, *Sci. Rep.*, 2017, **7**, 42525.

8 H. Cui, *et al.*, Synthesis of biodegradable and electroactive tetraaniline grafted poly(ester amide) copolymers for bone tissue engineering, *Biomacromolecules*, 2012, **13**, 2881–2889.

9 Q. Zhang, *et al.*, Electrical Stimulation with a Conductive Polymer Promotes Neurite Outgrowth and Synaptogenesis in Primary Cortical Neurons, *Sci. Rep.*, 2018, **8**, 1–10.

10 K. Roshanbinfar, *et al.*, Electroconductive Biohybrid Hydrogel for Enhanced Maturation and Beating Properties of Engineered Cardiac Tissues, *Adv. Funct. Mater.*, 2018, **28**, 1803951.

11 R. Balint, N. J. Cassidy and S. H. Cartmell, Conductive polymers: Towards a smart biomaterial for tissue engineering, *Acta Biomater.*, 2014, **10**, 2341–2353.

12 A. Ramanaviciene, A. Kausaite, S. Tautkus and A. Ramanavicius, Biocompatibility of polypyrrole particles: an *in vivo* study in mice, *J. Pharm. Pharmacol.*, 2007, **59**, 311–315.

13 J. Qu, X. Zhao, P. X. Ma and B. Guo, Injectable antibacterial conductive hydrogels with dual response to an electric field and pH for localized "smart" drug release, *Acta Biomater.*, 2018, **72**, 55–69.

14 X. Zhao, R. Dong, B. Guo and P. X. Ma, Dopamine-Incorporated Dual Bioactive Electroactive Shape Memory Polyurethane Elastomers with Physiological Shape Recovery Temperature, High Stretchability, and Enhanced C2C12 Myogenic Differentiation, *ACS Appl. Mater. Interfaces*, 2017, **9**, 29595–29611.

15 M. Li, *et al.*, Electroactive anti-oxidant polyurethane elastomers with shape memory property as non-adherent wound dressing to enhance wound healing, *Chem. Eng. J.*, 2019, **375**, 121999.

16 A. N. Zelikin, *et al.*, Erodible conducting polymers for potential biomedical applications, *Angew. Chem., Int. Ed.*, 2002, **41**, 141–144.

17 T. J. Rivers, T. W. Hudson and C. E. Schmidt, Synthesis of a novel, biodegradable electrically conducting polymer for biomedical applications, *Adv. Funct. Mater.*, 2002, **12**, 33–37.

18 L. Huang, *et al.*, Synthesis and characterization of electroactive and biodegradable ABA block copolymer of polylactide and aniline pentamer, *Biomaterials*, 2007, **28**, 1741–1751.

19 B. Guo, A. Finne-Wistrand and A. C. Albertsson, Universal two-step approach to degradable and electroactive block copolymers and networks from combined ring-opening polymerization and post-functionalization via oxidative coupling reactions, *Macromolecules*, 2011, **44**, 5227–5236.

20 B. Guo, L. Glavas and A. C. Albertsson, Biodegradable and electrically conducting polymers for biomedical applications, *Prog. Polym. Sci.*, 2013, **38**, 1263–1286.

21 T. Hu, *et al.*, Micropatterned, electroactive, and biodegradable poly(glycerol sebacate)-aniline trimer elastomer for cardiac tissue engineering, *Chem. Eng. J.*, 2019, **366**, 208–222.

22 Z. Deng, *et al.*, Stretchable degradable and electroactive shape memory copolymers with tunable recovery temperature enhance myogenic differentiation, *Acta Biomater.*, 2016, **46**, 234–244.

23 Y. Wu, L. Wang, B. Guo, Y. Shao and P. X. Ma, Electroactive biodegradable polyurethane significantly enhanced Schwann cells myelin gene expression and neurotrophin secretion for peripheral nerve tissue engineering, *Biomaterials*, 2016, **87**, 18–31.

24 L. Li, M. Yu, P. X. Ma and B. Guo, Electroactive degradable copolymers enhancing osteogenic differentiation from bone marrow derived mesenchymal stem cells, *J. Mater. Chem. B*, 2016, **4**, 471–481.

25 C. W. Hsiao, *et al.*, Electrical coupling of isolated cardiomyocyte clusters grown on aligned conductive nanofibrous meshes for their synchronized beating, *Biomaterials*, 2013, **34**, 1063–1072.

26 A. G. Guex, *et al.*, Electrospun aniline-tetramer-co-polycaprolactone fibers for conductive, biodegradable scaffolds, *MRS Commun.*, 2017, **7**, 375–382.

27 L. Ruiz-Cantu, *et al.*, Characterisation of the surface structure of 3D printed scaffolds for cell infiltration and surgical suturing, *Biofabrication*, 2016, **8**(1), 015016.

28 A. Prasopthum, M. Cooper, K. M. Shakesheff and J. Yang, Three-Dimensional Printed Scaffolds with Controlled Micro-/Nanoporous Surface Topography Direct Chondrogenic and Osteogenic Differentiation of Mesenchymal Stem Cells, *ACS Appl. Mater. Interfaces*, 2019, **11**, 18896–18906.

29 F. Gosselin, *et al.*, Solvent-Cast Three-Dimensional Printing of Multifunctional Microsystems, *Small*, 2013, **9**, 4118–4122.

30 A. Prasopthum, K. M. Shakesheff and J. Yang, Direct three-dimensional printing of polymeric scaffolds with nanofibrous topography, *Biofabrication*, 2018, **10**, 025002.

31 Y. J. Choi, *et al.*, 3D Cell Printing of Functional Skeletal Muscle Constructs Using Skeletal Muscle-Derived Bioink, *Adv. Healthcare Mater.*, 2016, **5**, 2636–2645.

32 C. E. Schmidt, V. R. Shastri, J. P. Vacanti and R. Langer, Stimulation of neurite outgrowth using an electrically conducting polymer, *Proc. Natl. Acad. Sci. U. S. A.*, 2002, **94**, 8948–8953.

33 A. S. Rowlands and J. J. Cooper-White, Directing phenotype of vascular smooth muscle cells using electrically stimulated conducting polymer, *Biomaterials*, 2008, **29**, 4510–4520.

34 R. D. Breukers, *et al.*, Creating conductive structures for cell growth: Growth and alignment of myogenic cell types on polythiophenes, *J. Biomed. Mater. Res., Part A*, 2010, **95**, 256–268.

35 A. F. Quigley, *et al.*, Electrical Stimulation of Myoblast Proliferation and Differentiation on Aligned Nanostructured Conductive Polymer Platforms, *Adv. Healthcare Mater.*, 2012, **1**, 801–808.

36 S. Meng, M. Rouabhia and Z. Zhang, Electrical stimulation modulates osteoblast proliferation and bone protein production through heparin-bioactivated conductive scaffolds, *Bioelectromagnetics*, 2013, **34**, 189–199.

37 Z. Liu, *et al.*, Mediation of cellular osteogenic differentiation through daily stimulation time based on polypyrrole planar electrodes, *Sci. Rep.*, 2017, **7**, 17926.

38 X. Zhao, B. Guo and P. X. Ma, Single component thermogelling electroactive hydrogels from poly(caprolactone)-poly(ethylene glycol)-poly(caprolactone)-graft-aniline tetramer amphiphilic copolymers, *J. Mater. Chem. B*, 2015, **3**, 8459–8468.

39 B. Guo, J. Qu, X. Zhao and M. Zhang, Degradable conductive self-healing hydrogels based on dextran-graft-tetraaniline and N-carboxyethyl chitosan as injectable carriers for myoblast cell therapy and muscle regeneration, *Acta Biomater.*, 2019, **84**, 180–193.

40 J. Qu, *et al.*, Degradable conductive injectable hydrogels as novel antibacterial, anti-oxidant wound dressings for wound healing, *Chem. Eng. J.*, 2019, **362**, 548–560.

41 N. Andronova, A. Finne and A. C. Albertsson, Fibrillar structure of resorbable microblock copolymers based on 1,5-dioxepan-2-one and ε-caprolactone, *J. Polym. Sci., Part A: Polym. Chem.*, 2003, **41**, 2412–2423.

42 G. P. Dowthwaite, *et al.*, The surface of articular cartilage contains a progenitor cell populations, *J. Cell Sci.*, 2004, **117**, 889–897.

43 L. Li, J. Ge, L. Wang, B. Guo and P. X. Ma, Electroactive nanofibrous biomimetic scaffolds by thermally induced phase separation, *J. Mater. Chem. B*, 2014, **2**, 6119–6130.

44 M. Xie, *et al.*, Ductile electroactive biodegradable hyperbranched polylactide copolymers enhancing myoblast differentiation, *Biomaterials*, 2015, **71**, 158–167.

45 R. Dong, X. Zhao, B. Guo and P. X. Ma, Self-Healing Conductive Injectable Hydrogels with Antibacterial Activity as Cell Delivery Carrier for Cardiac Cell Therapy, *ACS Appl. Mater. Interfaces*, 2016, **8**, 17138–17150.

46 Y. Liu, H. Cui, X. Zhuang, Y. Wei and X. Chen, Electrospinning of aniline pentamer-graft-gelatin/PLLA nanofibers for bone tissue engineering, *Acta Biomater.*, 2014, **10**, 5074–5080.
47 S. J. Leigh, R. J. Bradley, C. P. Purssell, D. R. Billson and D. A. Hutchins, A Simple, Low-Cost Conductive Composite Material for 3D Printing of Electronic Sensors, *PLoS One*, 2012, **7**, e49365.
48 G. Postiglione, G. Natale, G. Griffini, M. Levi and S. Turri, Conductive 3D microstructures by direct 3D printing of polymer/carbon nanotube nanocomposites via liquid deposition modeling, *Composites, Part A*, 2015, **76**, 110–114.
49 K. Gnanasekaran, *et al.*, 3D printing of CNT- and graphene-based conductive polymer nanocomposites by fused deposition modeling, *Appl. Mater. Today*, 2017, **9**, 21–28.
50 N. Annabi, *et al.*, Highly Elastic and Conductive Human-Based Protein Hybrid Hydrogels, *Adv. Mater.*, 2016, **28**, 40–49.
51 J. H. Collier, J. P. Camp, T. W. Hudson and C. E. Schmidt, Synthesis and characterization of polypyrrole-hyaluronic acid composite biomaterials for tissue engineering applications, *J. Biomed. Mater. Res.*, 2000, **50**, 574–584.
52 C. R. Broda, J. Y. Lee, S. Sirivisoot, C. E. Schmidt and B. S. Harrison, A chemically polymerized electrically conducting composite of polypyrrole nanoparticles and polyurethane for tissue engineering, *J. Biomed. Mater. Res., Part A*, 2011, **98A**, 509–516.
53 D. E. T. Shepherd and B. B. Seedhom, The 'instantaneous' compressive modulus of human articular cartilage in joints of the lower limb, *Rheumatology*, 1999, **38**, 124–132.
54 M. J. Higgins, P. J. Molino, Z. Yue and G. G. Wallace, Organic conducting polymer-protein interactions, *Chem. Mater.*, 2012, **24**, 828–839.
55 A. G. Macdiarmid and A. J. Epstein, Secondary doping: A new concept in conducting polymers, *Macromol. Symp.*, 1995, **98**, 835–842.
56 E. Ruoslahti and M. Pierschbacher, New perspectives in cell adhesion: RGD and integrins, *Science*, 1987, **238**, 491–497.
57 R. Jahn and D. Fasshauer, Molecular machines governing exocytosis of synaptic vesicles, *Nature*, 2012, **490**, 201–207.
58 J. G. Hardy, *et al.*, Electrical stimulation of human mesenchymal stem cells on biomineralized conducting polymers enhances their differentiation towards osteogenic outcomes, *J. Mater. Chem. B*, 2015, **3**, 8059–8064.
59 H. Castano, E. A. O'Rear, P. S. McFetridge and V. I. Sikavitsas, Polypyrrole thin films formed by admicellar polymerization support the osteogenic differentiation of mesenchymal stem cells, *Macromol. Biosci.*, 2004, **4**, 785–794.
60 H. J. Kwon, G. S. Lee and H. Chun, Electrical stimulation drives chondrogenesis of mesenchymal stem cells in the absence of exogenous growth factors, *Sci. Rep.*, 2016, **6**, 39302.
61 C. T. Jayasuriya and Q. Chen, Potential benefits and limitations of utilizing chondroprogenitors in cell-based cartilage therapy, *Connect. Tissue Res.*, 2015, **56**, 265–271.
62 Y. Jiang and R. S. Tuan, Origin and function of cartilage stem/progenitor cells in osteoarthritis, *Nat. Rev. Rheumatol.*, 2015, **11**, 206–212.
63 S. P. Ojanen, *et al.* Site-specific glycosaminoglycan content is better maintained in the pericellular matrix than the extracellular matrix in early post-traumatic osteoarthritis, *PLoS One*, 2018, **13**, e0196203.

